Defect-induced topological order-to-disorder transitions in two-dimensional binary substitutional solid solutions: A molecular dynamics study

Mo Li
Department of Materials Science and Engineering, The Johns Hopkins University, 3400 North Charles Street, Baltimore, Maryland 21218
(Received 25 May 2000)

The crystal to glass transition is investigated in two-dimensional Lennard-Jones random binary substitutional solid solutions using constant temperature and pressure molecular dynamics simulation. We find that defects generated by atomic size disorder are mainly dislocations and dislocation complexes. They are responsible for crystalline phase instability. The nature of the transition is shown to be determined by defect properties such as formation energy and density, and by kinetic constraints. We observe a continuous transition from crystal to glass with an intermediate hexatic phase characterized by short-range translational order and quasi-long-range orientational order. The implication of these results for melting and solid state amorphization is discussed.

I. INTRODUCTION

Melting is a well known example of topological order-to-disorder transition. At the melting point, the sharp Bragg peaks of crystalline phase suddenly become smeared out, signaling disappearance of the long-range translational symmetry. A less known but frequently occurring phenomenon is solid state amorphization (SSA), where crystalline solid becomes amorphous solid. The SSA is ubiquitous. It occurs in all types of crystalline solids and can be achieved through various means, including mechanical deformation, irradiation, solid state reaction, and hydrogen absorption.[1] Similar to melting, the SSA is characterized by disappearance of the Bragg peaks in crystalline phase at the transition. However, the disordered phase is amorphous solid. It is liquidlike, but does not have any long-range diffusion and does not show apparent viscous flow.

The SSA has attracted tremendous attention recently. It has been studied extensively in the past decade as a novel synthesis method to produce bulk amorphous materials. It is well understood now how the transition proceeds in different systems and under various conditions.[1] The current understanding is rooted in kinetics of the transformation. As pointed out by Johnson,[1] the necessary conditions for the SSA include the negative enthalpy of mixing of the elemental materials, highly asymmetric diffusivity, and the presence of structural defects. This understanding has resulted in successful prediction of new amorphous phases and rationalizing experimental results.[1–3] Very little is known, however, about microscopic mechanisms and thermodynamic nature of the transition.[1–4]

In most SSA the initial phases are unmixed elemental crystalline materials. The transformation to a chemically homogeneous amorphous phase needs to proceed by mixing these elements first. The transformation, therefore, occurs in highly heterogeneous environment, mostly by nucleation and growth of the amorphous phases at the interfaces, and other structural defects in the intermixing zone, or reaction front as in solid state reaction induced amorphization. As a result, kinetic factors, such as diffusion, interface and grain boundaries, dislocations, and solute miscibility, become critical to the transition. The prevalence of the kinetic effects in the SSA, set by the heterogeneous initial conditions, leads to the believe that the SSA is a first order transition.[1–3]

The question that has not been answered is how this transformation proceeds from the atomic point of view. More intriguing is the question of what the transition would look like if the inhomogeneity is removed. Since the free energy of a disordered solid such as an amorphous solid or glass is higher than that of the corresponding crystalline solid with the same composition, in order to transform the crystalline phase to amorphous solid, the free energy of the crystalline phase has to be raised to be equal or above that of the amorphous phase. Under isothermal condition, which is usually the case in most experiments, the increase of the free energy is caused by introduction of various types of disorder. For instance, mechanical attrition introduces dislocations, grain boundaries and other structure defects;[1,2] solid state reaction between two elemental metals introduces chemical as well as structural defects; and diffusion of hydrogen in rare-earth metals is believed to cause hydrogen interstitials and other complexities.[1–3] Clearly, these defects directly contribute to the instability of the crystalline phase. The phenomenology and the kinetics of different SSA induced by these defects have been understood and well documented. The wanted microscopic mechanism, therefore, needs to address the following question: How do these defects drive the crystalline phases unstable against amorphization?

The answer to this question is a fundamental one. It not only enhances our understanding of how the first order SSA proceeds in heterogeneous conditions, but also offers explanations and predictions for the SSA that could occur in homogeneous systems. It also has an important bearing on understanding of melting. The similar questions have been raised for the crystal to liquid transition: How do defects destroy the crystallinity? and would melting be the same (still be first order) if the heterogeneity such as free surfaces and interfaces are absent? The heterogeneity in melting, as in the SSA, is known as the cause for the nucleation of liquid phase. As these defects are always present, melting is a first order transition. As interfaces and free surfaces are reduced, the melting point is found to go up. The crystalline phase can therefore, be superheated considerably with reduced

preexiting heterogeneity.[5–8] The questions are what the limit of superheating is; what could be the nature of melting if this limit is reached; and finally, could melting as we know simply be a special case reduced from the phase transition intrinsic to crystalline instability?

As in the case of the SSA, these questions have not been answered for melting despite extensive efforts made in the past.[7,9–13] In this work, we aim at addressing some of these questions using model simulations. The model systems in our investigation are limited to those under isothermal conditions *below the glass transition temperature*. Although this is the setting typical for the SSA, it opens a new dimension for understanding of crystalline instability that is not accessible for melting. Defects in this model system can be introduced into crystals through various means other than by thermal agitation. Thus temperature becomes an additional parameter that can be used to control the state of the defects. As we show later, the SSA can be considered a melting transition driven by the frozen defects. By comparing the SSA and melting, we can learn a great deal about the nature of topological order-to-disorder transitions.

This paper is organized as following. In Sec. II, we describe briefly some important features of the model system and simulation methods. Some physical quantities employed to characterize different phases and transitions will also be explained. In Sec. III, we present results for two model systems of binary solid solutions. One is kept under a constant atomic size difference between two types of atoms, while the solute concentrations are varied. Another has its concentration fixed, while the atomic sizes change. We show that these systems possess the same types of topological defects but different characteristics in the order parameters and different nature for the transitions. In Sec. IV, we discuss these results and compare them with those in melting. In Sec. V, we summarize the results presented in this paper.

II. MODEL AND COMPUTATION METHOD

A. Model

In this work, we use a binary substitutional solid solution model to study defects and the SSA. The reason for this choice is as follows.

(1) It is convenient to generate defects and to create an environment free of preexisting inhomogeneities (free surfaces, interfaces, grain boundaries, and dislocations). By simply varying *atomic size difference* of the two constituent components, we can obtain a variety of topological defects such as disclinations, dislocations, and grain boundaries. (2) The amorphous phase formed in the binary system, as compared with monoatomic system, is stable at temperatures close to the glass transition temperature ($T<T_g$). It gives us a large time window to measure dynamic and thermodynamic properties. (3) This binary solid solution model represents a large class of systems that are known from experiments undergoing SSA. In cases such as solid state reaction induced SSA, hydrogen absorption induced SSA, and irradiation induced SSA, metastable crystalline solid solutions form before and during SSA.[1] In general, one can consider the formation of solid solution in the crystalline phase as a necessary precursor to the polymorphic amorphization transition. Therefore, without losing generality, the solid solution model serves as a simplest model system for understanding crystalline instability in SSA.

In this work, we focus our attention only on the topological-order-to-disorder transition in two-dimensional (2D) binary solid solutions because it is convenient to generate and characterize various defects in 2D. Furthermore, the large number of theoretical work and computer simulations on 2D melting[9,14,15] offer a rich set of references that can be used to compare with our work.

The model system of the binary random substitutional solid solutions consists of two types of atoms that interact with Lennard-Jones (LJ) potentials (1a). To ensure that they go to zero smoothly at the finite cutoffs r_c (1b), LJ potentials are modified by using a cubic spline switch function:[16]

$$\phi(r)=-4\epsilon_{\alpha\beta}\left[\left(\frac{\sigma_{\alpha\beta}}{r}\right)^{12}-\left(\frac{\sigma_{\alpha\beta}}{r}\right)^{6}\right]S(r), \tag{1a}$$

$$S(r)=\begin{cases}1, & r\leqslant r_l,\\ 1-\dfrac{(r-r_l)^2(3r_c-r_l-2r)}{(r_c-r_l)^3}, & r_l<r<r_c,\\ 0, & r\geqslant r_c\end{cases}, \tag{1b}$$

where α and β denote the two atomic species (A and B). The cutoffs are $r_c=2.45\sigma$, and $r_l=1.90\sigma$, where σ is defined below. r_c is roughly between the fourth and fifth nearest neighbors, respectively.

For the potential depth, we use the same value for all interatomic interactions in the binary solid solution,

$$\epsilon_{\alpha\beta}=\epsilon, \tag{2}$$

for α, $\beta=A,B$, but different atomic sizes,

$$\sigma_{AA}=\sigma,$$

$$\sigma_{BB}=\alpha\sigma_{AA}=\alpha\sigma, \tag{3}$$

$$\sigma_{AB}=\frac{1}{2}(\sigma_{AA}+\sigma_{BB})=\frac{1}{2}(1+\alpha)\sigma,$$

where the parameter

$$\alpha=\frac{\sigma_{BB}}{\sigma_{AA}} \tag{4}$$

is the atomic size ratio between the solute atoms (denoted as B), and the solvent atoms (denoted as A). Therefore, only two parameters, ϵ and α, are used to parametrize the LJ interactions.

The potentials with the same depths could avoid such phenomena as chemical short-range ordering, or clustering. These unwanted complications could obscure the results for SSA. At a given temperature and pressure, the 2D binary solid solutions are completely determined by only two parameters, α, and the concentration x of the solute atoms B,

$$x=\frac{N_B}{N_{\text{total}}}=\frac{N_B}{N_B+N_A}, \tag{5}$$

where N_B and N_A are the number of solute and solvent atoms and N_{total} is the total number of atoms in the system.

To simplify the model further, we set the mass of both types of atoms to be equal, $m_A = m_B = m$. This choice might have some consequences in the transport properties. But our system is kept at sufficiently low temperatures so that long-range atomic migration is absent. Therefore, the effect of this choice is insignificant. All quantities calculated in this model are expressed in reduced LJ units, scaled by two parameters, σ and ϵ. For instance, temperature is in the units of ϵ/k_B and time has the units $\sqrt{(m\sigma^2/\epsilon)}$.

B. Computation procedure

Atomic configurations, thermodynamic properties, and dynamic properties of the model system are obtained using constant temperature and pressure molecular dynamics simulation method. Details of the simulation technique can be found in Refs. 17 and 18. The computation procedures unique for the binary random arrays are briefly described below.

Starting from a pure LJ crystal made of bigger atoms A on the hexagonal lattice, we prepared the substitutional binary solid solutions in two ways. One is to replace the big atoms randomly by the smaller atoms B with the relative concentration x at each given atomic size ratio α. Each new solid solution is generated from the previous one by gradually increasing the solute concentration x. In the present work, we chose to increase x by 2.5% each time a new solid solution was generated. The second method is to vary α of the binary mixtures at a given x. Starting from the pure LJ crystalline solid, each new solid solution is generated from the previous one by decreasing α by 0.05. No significant difference is found for the samples with the same x and α prepared via two different paths.

The smallest α used in this work is 0.7 at which the binary solid solution can still remain homogeneous without formation of short-range order or cluster. Further reduction of α may result in undesired local packing where too small solute atoms might be trapped in the interstitial positions of larger solvent atoms, or some ordered configurations similar to intermetallic compounds might be favored. We should point out that it is equally valid to chose large atoms as solute and small ones as solvent, and the results should remain the same.

To maintain chemical homogeneity, or polymorphism at the transition, we need to prevent long range diffusion from occurring. To do it, we keep the binary arrays below the liquid-to-glass transition temperature T_g. At such low temperatures, it is difficult for both solvent and solute atoms to diffuse. As a result, defects cannot migrate afar to form aggregates. Here T_g is determined previously by quenching the corresponding binary liquids using constant pressure MD with a quench rate of 10^6 K/s. T_g was found to be almost a constant for different binary arrays with the same atomic size ratio but different concentrations.

Since the binary arrays are kept below liquid to glass transition temperature, long simulation time is required to reach equilibrium and then to obtain physical properties. Typically, 10^{5-6} MD steps are used for equilibration and an equal number of steps are used to collect physical properties. Close to the crystal to glass transition, 10^7 MD steps are used. This corresponds to a few hundred nanoseconds for the LJ parameters of argon. The sample size also varys depending on how close the system is to the amorphization transition. Typically 5000–8000 atoms are used close to the transition, and smaller systems with a few thousands of atoms are used for ordered phases.

In addition to time averages, we also performed configuration averages to obtain thermodynamic properties for the random solid solutions. This ensures the reliability of our results for different arrays with different initial random solute distribution with finite sample sizes. We normally took 5 to 10 different configurations to obtain the configuration average for each solution with the same values of α and x but different initial solute distributions.

C. Defects

The simplest structural defect in 2D is disclination. Dislocations in 2D are composed of two nearest neighbor disclinations, one positive and one negative.[19,20] To reduce long range elastic energy, dislocations form pairs with two dislocations of opposite Burgers vectors. When a large number of dislocations are present, or if they are sufficiently mobile, they tend to form more complicated defects such as grain boundaries in order to reduce the elastic energy resulting from their mutual interactions.[21] The successive occurrence of different types of defects starting from elementary disclinations, to dislocations, and to other more complicated defect aggregates are determined by both strain energy and elemental defect density. We show in Sec. III A 3 that one particular type of defect complex in the binary solid solutions, the short chain of dislocations, plays a very important role in the SSA. The large, connected chains form grain boundaries.[21]

In 2D, dislocations, grain boundaries, and dislocation complexes made of the two types of elemental disclinations can be identified by mapping out the nearest neighbor coordinates of each atom.[19,20] The coordination numbers of an atom are accounted usually using the Voronoi polyhedron construction that locates the minimum volume polyhedron for each atom with each face bisecting the atomic bonds linking the nearest neighbor atoms. In binary arrays consisting of different types of atoms of very different sizes, we use the radical plane method developed by Fisher and Koch.[22] Because of the difference in atomic size, the polyhedron determined by simply bisecting atomic bonds using Voronoi method may not be minimal. The radical plane method accounts adequately for the atomic size difference in determining the nearest neighbor atoms.

D. Translational and orientational order

A general relationship between translational and orientational symmetry and crystalline defects is proposed in the theory of 2D melting by Kosterlitz, Thouless,[23] Nelson, Halperin,[24] and Young[25] (KTNHY). According to this theory, melting occurs when dislocation-pairs, presumably generated by thermal agitation, start unbinding. The surviving orientational order is destroyed later as further unbinding of dislocation singlets into isolated disclinations.[24] The ''hexatic phase'' is a liquid-crystal-like phase characterized

by short-range translational symmetry and quasi-long-ranged orientational symmetry. Although conflicting results still remain as for the exact nature of 2D melting,[9,14,15,26,27] general concepts such as translational and orientational order and its relation to defects have provided a powerful tool for analyzing topological order-to-disorder transitions in 2D. We shall use this approach in this work to assess crystalline disorder in the 2D solid solutions.

The translational order parameter is defined as

$$\rho_{\mathbf{G}}(\mathbf{r}) = e^{i\mathbf{G}\cdot\mathbf{r}}, \tag{6}$$

where $\mathbf{r}$ is the atom position and $\mathbf{G}$ is chosen as the shortest reciprocal lattice of the hexagonal lattice (corresponding to the first Bragg peak position). As Nelson *et al.*[24,27,28] pointed out, the translational symmetry is most susceptible to the presence of dislocations, stacking faults, and grain boundaries. The orientational order parameter is defined as

$$\rho m(\mathbf{r}) = e^{im\theta(\mathbf{r})}, \tag{7}$$

where $\theta(\mathbf{r})$ is the angle of the bond between the atom and its nearest neighbor with respect to a reference axis. Here $m=6$ for a hexagonal lattice and $m=4$ for a system with square symmetry. Orientational symmetry is less susceptible to dislocations and stacking faults; it is disturbed instead by disclinations and grain boundaries.

The correlation functions of these symmetry order parameters are

$$C_{\mathbf{G}}(r) = \langle\langle \rho^*_{\mathbf{G}}(\mathbf{r})\rho_{\mathbf{G}}(0)\rangle\rangle \tag{8}$$

and

$$C_m(r) = \langle\langle \rho^*_m(\mathbf{r})\rho m(0)\rangle\rangle, \tag{9}$$

where $\langle\langle\cdots\rangle\rangle$ denotes the time and configuration averaging. From the correlation lengths of these correlation functions, one can measure the spatial extension of both kinds of order. For a crystalline phase, both order correlation functions are long-ranged. In 2D, the long-range translational correlations are destroyed by fluctuations of the long wavelength phonon modes, making the translational symmetry quasi-long-ranged.[24] The translational correlation function decays in a power law fashion over distance. For a liquid or amorphous phase, both order correlation functions are short-ranged and manifested in an exponential decay. The hexatic phase, on the other hand, is characterized by a short-range translational symmetry and quasi-long-range orientational symmetry.

Besides the order correlation functions, we also compute the local order parameters defined as averages of the order parameter over the entire sample,[29]

$$LTO = \frac{1}{N_{\text{total}}}\sum_i^{N_{\text{total}}} \rho_{\mathbf{G}}(\mathbf{r}_i) \tag{10}$$

and

$$LOO = \frac{1}{N_{\text{total}}}\sum_i^{N_{\text{total}}}\left[\frac{1}{N_i}\sum_j^{N_i}\rho m(\mathbf{r}_j)\right], \tag{11}$$

where N_i is the number of the nearest neighbors of the ith atom. Here *LTO* and *LOO* stand for local translational order and local orientational order. Both *LTO* and *LOO* are close to unity in a crystalline phase, and become nearly zero in a liquid or amorphous phase. A hexatic phase has a nearly zero *LTO* but finite *LOO*.

E. Atomic displacements

Both melting and SSA are topological order-to-disorder transition involving changes in atomic positions from a topological ordered phase to disordered one. This change is measured quantitatively by the atomic displacement field defined as

$$\mathbf{u}_i = \mathbf{r}_i - \mathbf{R}_i = \mathbf{u}_i^d + \mathbf{u}_i^s, \tag{12}$$

where $\mathbf{r}_i$ is the instantaneous position of the ith atom and $\mathbf{R}_i$ is its position in a perfect crystalline, or ordered phase; $\mathbf{u}_i^d$ is the dynamic displacement arising from thermal vibrations of the atom around the mean atomic position; and $\mathbf{u}_i^s$ is the static displacement from the ordered positions caused by various structural defects. Both quantities contribute to the Debye-Waller factor describing the broadening of the Bragg peaks of crystalline phases.

The dynamic displacement fields can be written as

$$\mathbf{u}_i^d = \mathbf{r}_i - \langle\mathbf{r}_i\rangle, \tag{13}$$

where $\langle\cdots\rangle$ stands for time average, and $\langle\mathbf{r}_i\rangle$ is the mean atom position averaged over many configurations due to thermal vibration. The static displacement field is written as

$$\mathbf{u}_i^s = \langle\mathbf{r}_i\rangle - \mathbf{R}_i. \tag{14}$$

$\mathbf{R}_i$ is the atomic position of the reference lattice with the same density as the disordered one. (Otherwise an additional displacement needs to be added to account for changes in lattice parameter. However, such uniform change in lattice parameter is irrelevant to representing topological order to disorder transition.)

The degree of atomic position disorder can be measured by the mean values of the atomic displacements. The dynamic and static mean square atomic displacements (MSD) are written as

$$\langle(\delta\mathbf{u}^d)^2\rangle = \frac{1}{N_{\text{total}}}\sum_i^{N_{\text{total}}}\langle(\mathbf{u}_i^d)^2\rangle \tag{15}$$

and

$$\langle(\delta\mathbf{u}^s)^2\rangle = \frac{1}{N_{\text{total}}}\sum_i^{N_{\text{total}}}(\mathbf{u}_i^s)^2. \tag{16}$$

Equation (15) is the familiar one used by Lindemann to predict the onset of melting.[12] We will use the mean static displacement (16) to measure the disorder in SSA caused by defects.

III. RESULTS

Some relevant thermodynamic state variables and physical properties are briefly described below for the substitutional random binary arrays:

The melting temperature of the pure 2D LJ crystal at zero external pressure is found to be 0.41–0.43, which is in agree-

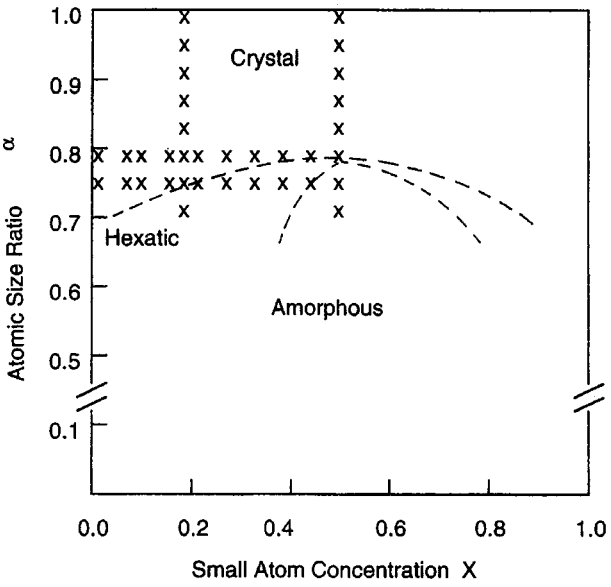

FIG. 1. Phase diagram of the two-dimensional binary random substitutional solid solutions at $T=0.20$ and $P=0.0$. Cross signs mark the systems that were actually simulated.

ment with the previous work.[9] With the quenching rate of 10^6 K/s, we find the glass transition temperature for the pure LJ liquid between 0.22 and 0.25. As x increases the melting temperature decreases from the pure LJ values while the glass transition temperature remains almost constant.

The binary arrays are characterized by four state variables, temperature T, external pressure P, the solute concentration x, and the atomic size ratio α. Practically, it is almost impossible to study all systems specified by these parameters. To be as representative as possible, the parameters that can best serve our purpose are as follows.

Throughout our simulation, we take $P=0$ and $T=0.20(<T_g)$ for all systems studied. For the given pressure and temperature, the binary arrays are simulated along two paths specified by x and α. The first is to vary solute concentration α at a given atomic size ratio x, and the second is to vary atomic size ratio α at a given solute concentration x. Figure 1 shows the atomic size-solute concentration phase diagram for the systems studied. Several topologically disordered phases are shown at different atomic size ratios and solute concentrations. There is a critical atomic size difference, $\alpha\approx 0.825$, *above* which only crystalline phases exist (see Fig. 1). In the following section, we will present results from one of the binary arrays with atomic size ratio at $\alpha=0.75$ and varying solute concentrations.

A. Binary arrays with $(x,\alpha=0.75)$ at $T=0.20$, $P=0.0$

1. Structure

As shown in Fig. 2, the structural evolution of the binary arrays can be seen from their radial distribution functions (RDF). The RDF shows that the binary arrays become more and more disordered as we gradually increase the solute concentration. As the solute concentration increases, all peaks of the RDF becomes broadened and the ones at large distances become flattened first. A quantitative change of the RDF occurs at $x=0.20$ where the peaks of RDF become smeared

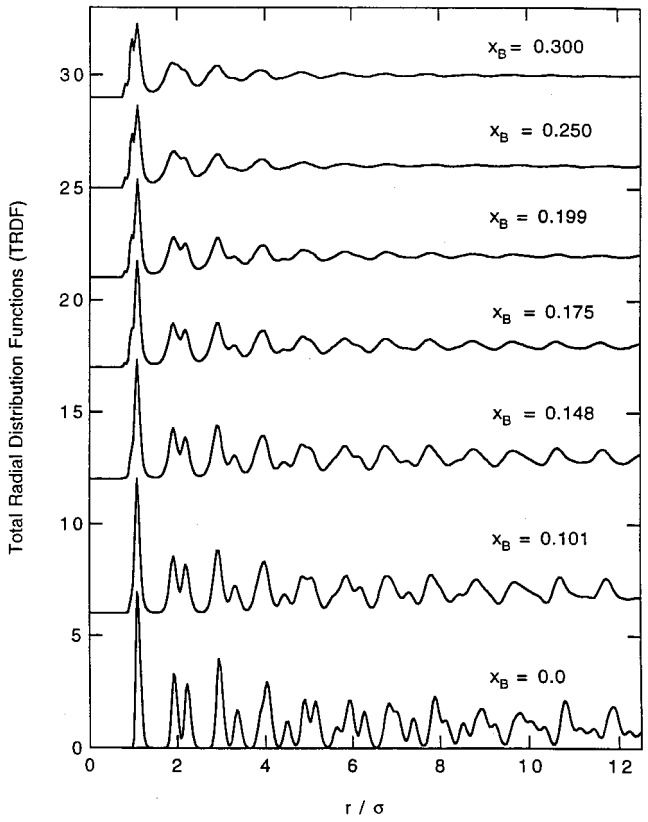

FIG. 2. Radial distribution functions (RDF) for two-dimensional arrays with $\alpha=0.75$, at $T=0.20$ and $P=0.0$.

at distances beyond the fourth nearest neighbors. Further increasing of solute concentration does not change the RDF quantitatively.

Amorphous phase with isotropic interatomic interactions is often identified by the split-second peaks in the RDF. However, in 2D hexagonal lattice, the second and third peaks in the RDF are very close (see the RDF at $x=0$), a feature that is retained even in the amorphous phase. Therefore, this criterion cannot be used to identify the amorphous phases formed from the hexagonal crystalline phase. The partial RDF are not useful either since the second and third peaks are even more persistent. Although an alternative method was proposed by Wong and Chester[30] to identify the second-split peaks for 2D glasses from rapid quenched liquids, our results suggest that other methods should be considered.

The most straightforward method is to map out the atomic configurations. It is particularly suitable to a 2D glass. Problems may arise regarding the reliability of such method, since there is no true long-range translational order in two dimensions.[24] In practice, this concern is essentially unnecessary.[9] Figure 3 shows the snapshots of the atomic configurations of the binary arrays at different solute concentrations.

The atomic configurations show that the binary arrays do maintain their crystallinity up until $x=0.20$, where the amorphous phases start forming. Above $x=0.20$ we see that the amorphous phase actually contains tortuous crystal-like regions interweaved with disordered regions. This feature is specially noticeable in the concentration range between $x=0.25-0.30$. Each of the crystalline regions retains hexago-

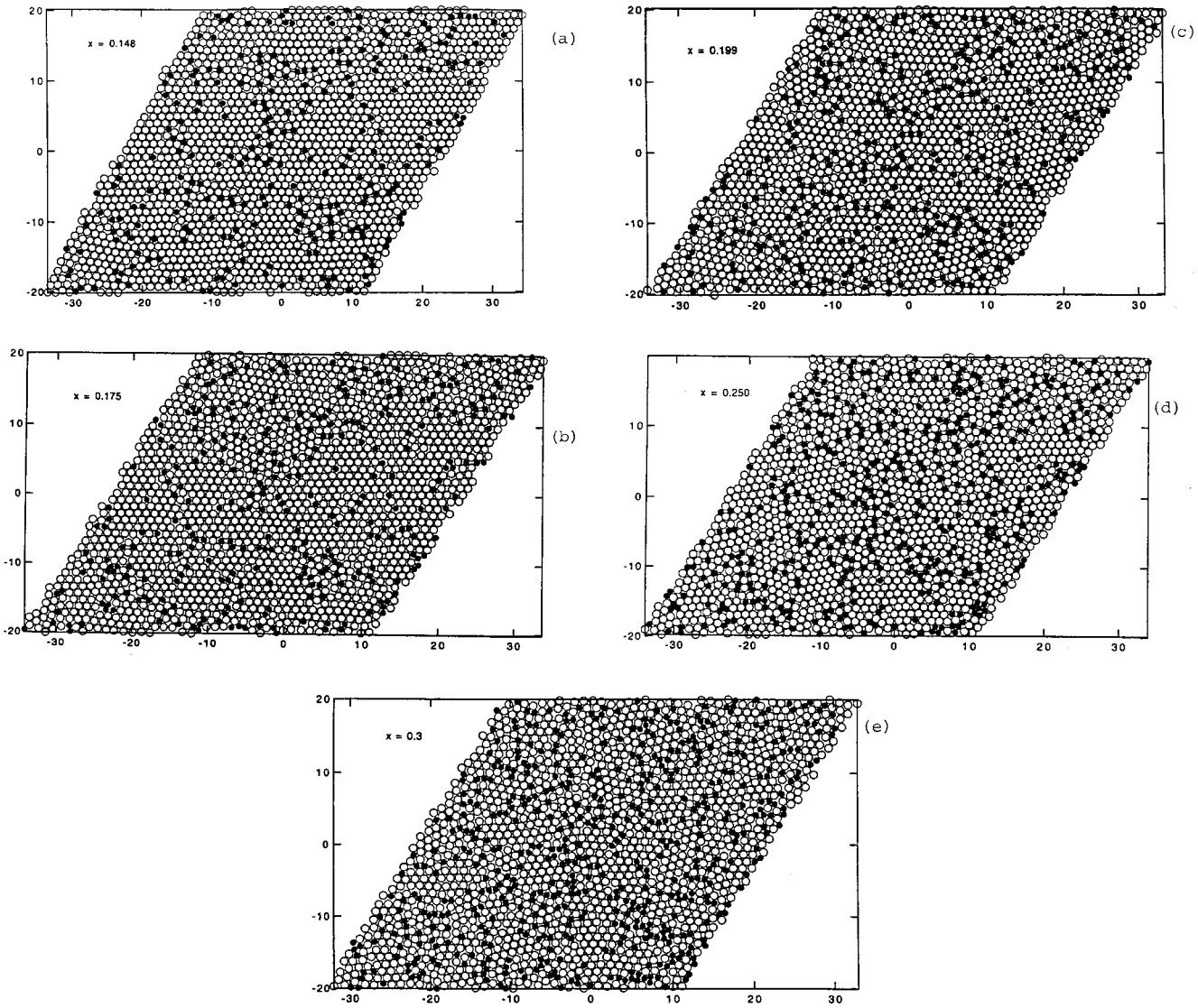

FIG. 3. Atomic configurations of the two-dimensional binary arrays with $\alpha = 0.75$, at $T = 0.20$ and $P = 0.0$. Circles are solvent atoms and filled circles are solute atoms.

nal symmetry of the parent crystalline phase but differs most obviously in their relative orientations. Their sizes range on average from ten to a few hundred atoms across. The average sizes of these regions become smaller with increasing solute concentration. It appears that the disordering occurs via a mechanism of fragmentation of the parent crystalline phase by addition of solute atoms. In the following sections, we will explore the connections between this mechanism and various defects present in the binary arrays.

2. Order, correlation functions, and hexatic phases

More detailed structural features exhibited by the various phases of the binary arrays are revealed by the translational and orientational order parameters and their correlation functions. In Fig. 4, we plot the average LTO and LOO for the binary arrays. Both order parameters decrease slowly with increasing solute concentration until $x = 0.15$. Beyond this point, they start to decline dramatically. The LTO decreases faster. At $x = 0.20$ where the amorphous phase was shown to form, the LTO already becomes nearly zero, typical for a

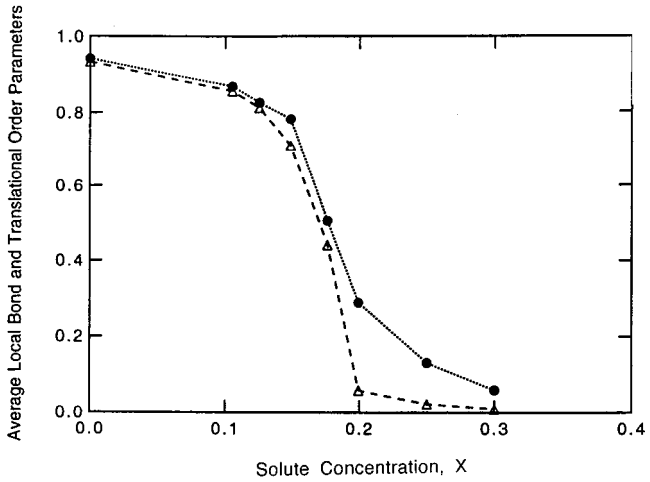

FIG. 4. Average local translational and orientational order parameters for binary arrays with $\alpha = 0.75$ at $T = 0.20$ and $P = 0.0$. Triangles denote the translational order and filled circles denote the orientational order.

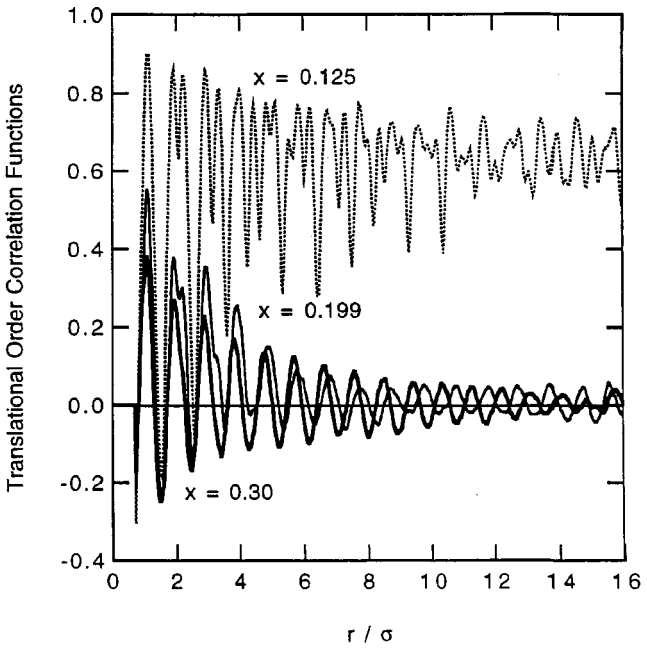

FIG. 5. The translational order correlation functions for binary arrays with $\alpha=0.75$ at $T=0.20$ and $P=0.0$.

liquid. But the LOO still remains at a relatively large value and vanishes only later at $x=0.40$. The amorphous phases between $x=0.20-0.40$ are characterized by absence of the long-range translational order and finite orientational order, suggesting the existence of a hexatic amorphous phase.[24,28,31]

Figures 5 and 6 show the translational and bond orientational order correlation functions as defined in Eqs. (8) and (9). The translational order correlation function for a pure LJ solid is long-range, but apparently decays over distance. Such behavior is characteristic of 2D crystals. This quasi-long-range decay of the translational order correlation function is caused by fluctuations of the long wavelength

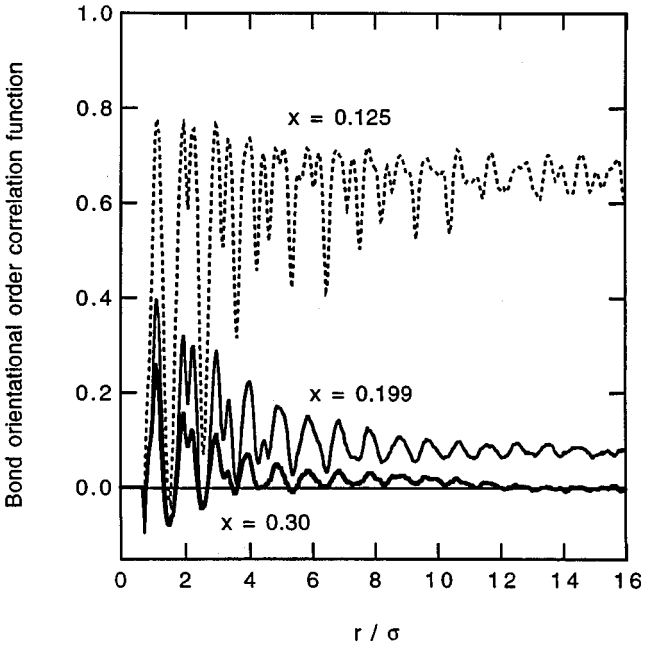

FIG. 6. The bond orientational order correlation functions for binary arrays with $\alpha=0.75$ at $T=0.20$ and $P=0.0$.

phonons that spontaneously destroy the true long-range translational order. In contrast, the bond orientational order correlation function of the pure LJ solid stays constant over distance, indicating that the orientational order is truly long-range.

Increasing the solute concentration leads to further decay in the translational correlation functions. The correlation lengths associated with these translational correlation functions at different solute concentrations remain quasi-long-range. At $x\geqslant 0.20$, where the RDF in Fig. 2 as well as the LTO in Fig. 4 show the onset of the amorphous phase, the translational correlation function approaches zero at distances of about the fourth and fifth nearest neighbors. Further increase of solute concentration beyond this point results in translational correlation functions showing no crystalline features but over damped oscillations. The correlation lengths match the average size of the crystal-like regions observed in the atomic configuration in Fig. 3.

The orientational order correlation function behaves quite differently. As more solute atoms are added, it begins to show the familiar quasi-long-range decay, but much slower than the translational order correlation function. Of particular interest is that in the concentration range above 0.20 where amorphous phase appears, the orientational order correlation functions still maintain the familiar quasi-long-range behavior. This correlates well with the behavior of the LOO shown in Fig. 4. Such persistent orientational order starts to fade only at much higher solute concentrations ($x\geqslant 0.40$), where the orientational correlation function becomes short-range.

The amorphous phase between $0.20\leqslant x\leqslant 0.30$ characterized by short-range translational order and quasi-long-range orientational order could well be the hexatic phase.[24,28] A careful inspection of the atomic configurations (to obtain the best result, the reader is advised to view these configurations from directions at a small inclined angle away from the paper; translational and orientational symmetry breaking can be perceived the best in this way by rotating the figures about the normal of the paper), reveals that in the concentration range between 0.20 and 0.40, the crystal-like regions show a much less abrupt change in the *relative orientation* than in the translational order. Beyond the distance corresponding to the translation correlation length defining the size of the crystalline fragments, the atomic lines (corresponding to atomic planes in three dimensions) in the crystal-like regions terminate suddenly at the edges of the domains where extra atomic lines emerge (which are edge dislocations in 3D). The relative rotation of these atomic lines from one crystal-like region to its adjacent ones changes, however, relatively smoothly.

According to the KTNHY theory of 2D melting, the hexatic phase forms as a result of unbinding of dislocation pairs into dislocation singlets. These dislocation singlets destroy translational order but leave orientational order intact. Indeed, the detailed defect configurations, as shown in the next section, exhibit such behavior.

Finally, to eliminate any concern that the intermediate hexaticlike phases are transient phases resulting from possible hysteresis and slow kinetics, all simulations for binary arrays having solute concentrations at or close to the hexatic region were done with exceedingly long equilibration times (typically 10^{7-8} MD steps). Based on the results obtained

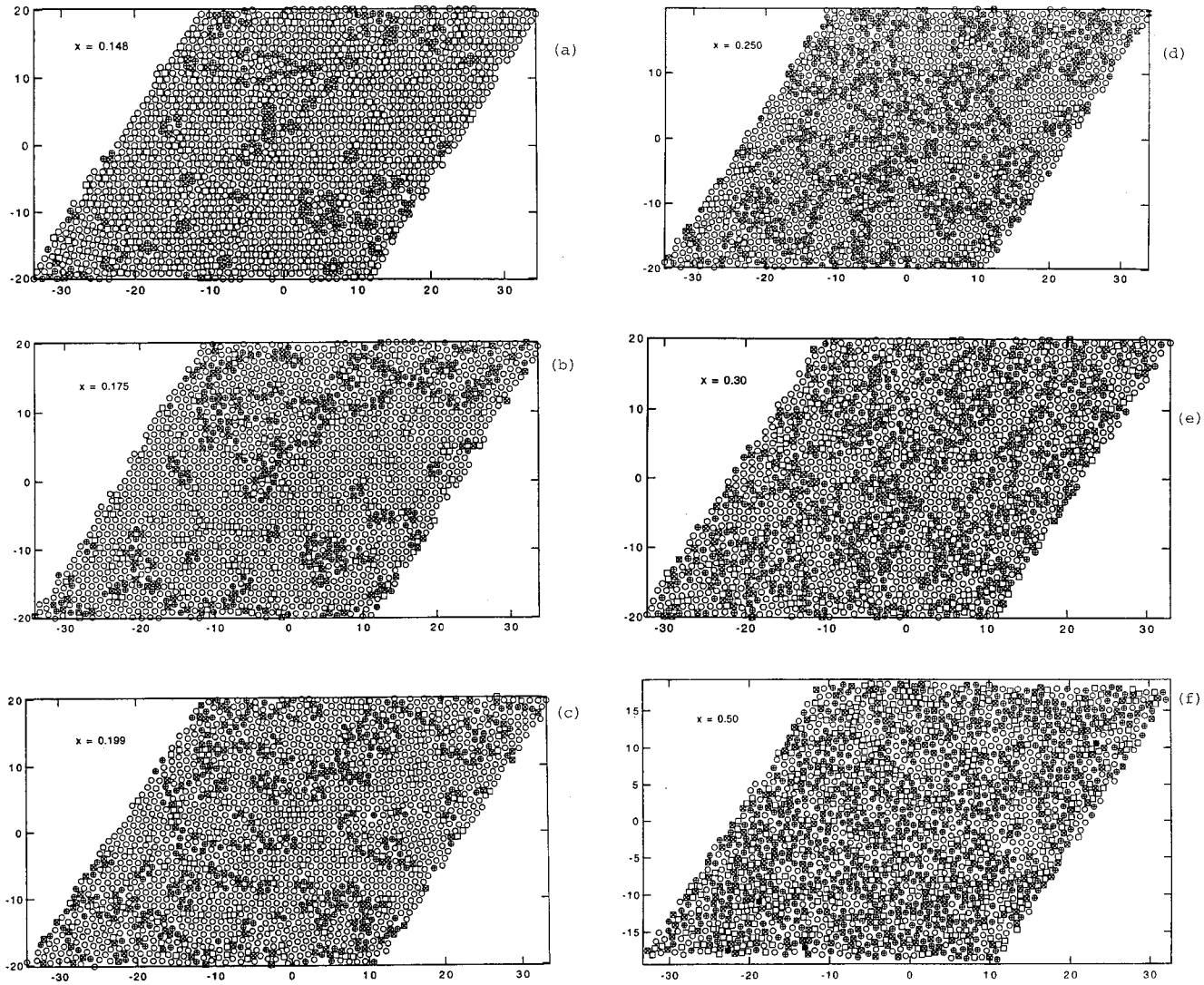

FIG. 7. The atomic configurations of defects in the binary arrays with $\alpha = 0.75$ at $T = 0.20$ and $P = 0.0$. Triangles represent disclinations with four nearest neighbors, crosses represent disclinations with five nearest neighbors, plus signs represent seven nearest neighbor disclinations, and asterisks represent eight nearest neighbor disclinations. A 5 NN and a 7 NN disclination separated by a lattice spacing forms a single dislocation. To present a better view of defect, we use squares to represent solute atoms and circles for solvent atoms. Note the overwhelming number of dislocation pairs in the binary arrays that always have two solute-solvent pairs (two circles and two squares).

thus far, we conclude that the intermediate hexatic phase is indeed a unique phase for 2D binary LJ solid solutions.

3. Defects

Using the technique described in Sec. II C, we mapped out various defect configurations at different solute concentrations. As shown in Fig. 7, there are many interesting features exhibited in the defect configurations.

First, the defects are generated exclusively by atomic size differences between the solvent and solute atoms. Defects always occur at or around the solute atoms. The smaller solute atoms that induce defects always have five-nearest neighbor disclinations; and the solvent atoms have seven-nearest neighbor ones.

Second, dislocations always form pairs in the crystalline phases so as to reduce the elastic energy from the long-range elastic strain fields associated with the dislocation singlets. We have found only a neglectable number of isolated dislocations composed of a negative and a positive disclination pair in the binary arrays. As the solute concentration increases, especially beyond $x = 0.20$, we find that dislocations tend to form more complicated configurations, presumably for the same reason of reducing elastic energy. As shown in Fig. 7, they appear as chains made of elongated dislocation singlets and pairs, or dipoles. As the solute concentration increases further, the chainlike clusters become connected: and at higher concentrations, they grow into the rest of the crystalline regions, and gradually lose their identity.

These dislocation network defects cannot be considered as grain boundaries yet because their scales are only microscopic. The sizes of the chainlike dislocation segments range from a few atomic spacings in the binary arrays with low solute concentrations ($x = 0.0$ to 0.15) to a few hundred atomic spacings at high solute concentrations ($x = 0.20$ to 0.50). Furthermore, they do not form closed loops in the crystalline phase until very high density of dislocations is reached ($x > 0.25$). We therefore, prefer to call them *dislocation network chains*. They are apparently the precursor of

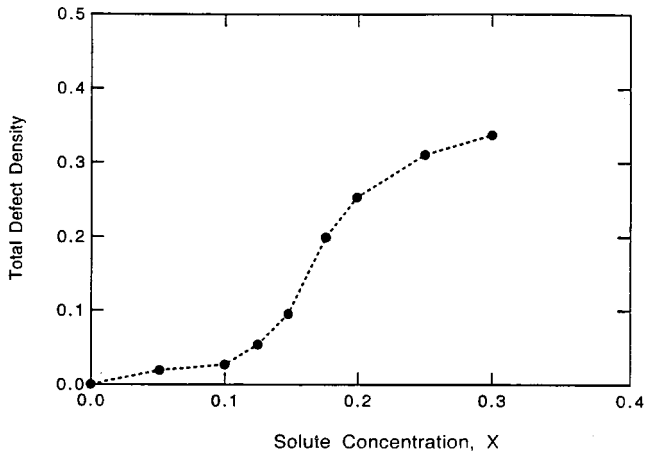

FIG. 8. The average defect density of the binary array with $\alpha = 0.75$ at $T = 0.2$ and $P = 0.0$.

grain boundaries made of elongated edge dislocations dipoles in 2D caused by the characteristic interactions between edge dislocations. The SSA transition in 2D is closely related to this type of defect.

The average defect density calculated for the binary arrays is presented in Fig. 8. It is summed over the atoms at the cores of disclinations and divided by the total number of atoms. Since most disclinations are five- and seven-nearest neighbor disclinations that occur in pairs (with few four- or eight-nearest neighbor disclinations), a half of the density is that of the dislocations. Similarly, one fourth of the disclination density is the dislocation pair density.

The defect density rises at $x = 0.15$, prior to which the only defects are dislocation pairs. At the onset of the amorphization ($x = 0.20$), the total disclination density reaches approximately 25%, or 13% of dislocations. If we divide this density by the total area of the samples, we get the dislocation density in the order of $10^{12}\,\mathrm{nm}^{-2}$ which is typical for severely deformed metals.[21] Incidentally, this value is also close to the critical density in order to induce melting.[32]

Furthermore, a careful observation of the defect configurations in Fig. 7 reveals that the defects in the binary arrays at $x = 0.20$ are quantitatively different. The tightly bonded dislocation pairs start breaking loose. Some form isolated dislocation singlets while others become elongated to form short dislocation network chains. Defining the isolated dislocations as those that are separated by at least one lattice spacing, we find that at the hexatic phase transition roughly 15% of the total number of dislocations are singlets; and approximately an equal number of dislocations are in the dislocation network chains. If we count the dislocations in short dislocation network chains as isolated dislocations (because of their severe elongation), the density of isolated dislocations reaches 25–30 %. This large number of separated dislocation singlets at $x = 0.20$ provides a strong evidence of formation of a hexatic phase.

4. Elastic behavior

Because of their important roles in characterizing instability of crystalline phase as pioneered by Born,[1,3,4,11] the elastic constants of the binary arrays have also been investigated (Fig. 9).

Since the 2D hexagonal crystalline phase and the amorphous phase are both isotropic, the condition of elastic isotropy, $C_{44} = (C_{12} - C_{44})/2$, reduces the total number of independent elastic constants to two. They are usually expressed

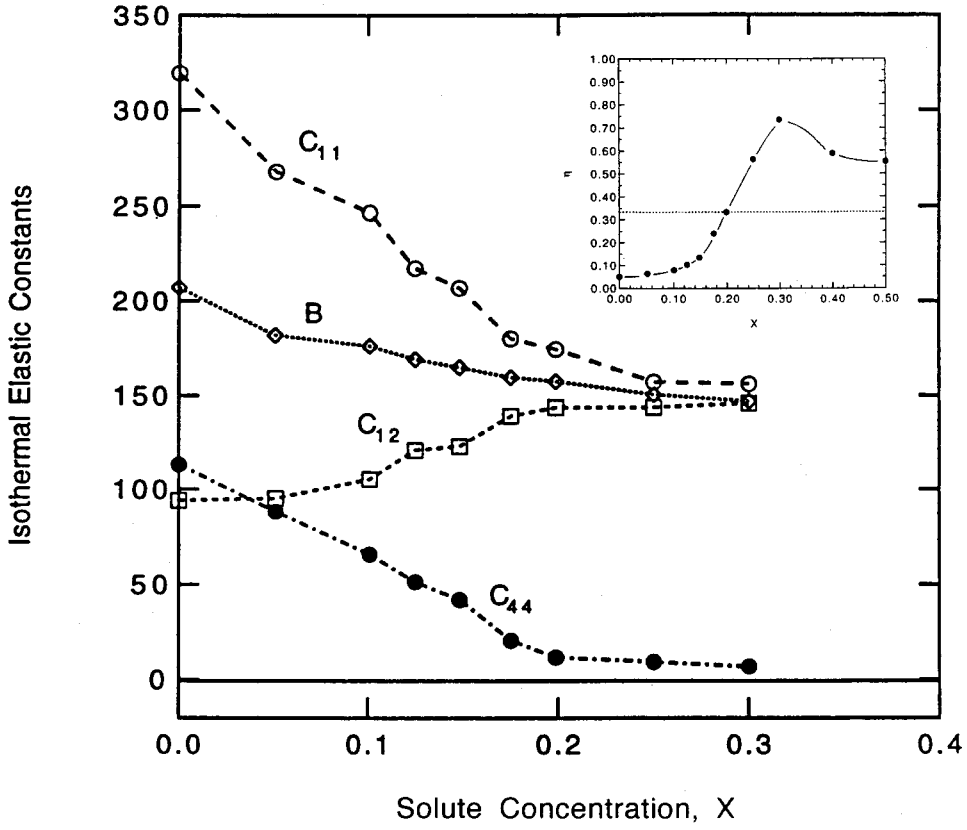

FIG. 9. Isothermal elastic constants versus solute concentration in the binary arrays with $\alpha = 0.75$ at $T = 0.20$ and $P = 0.0$. They are all in units of $N_{\mathrm{total}} k_B T/A$, where A is the equilibrium area of each binary array. The inset is the Poisson ratio.

as Lamé coefficient, $\lambda = C_{12}$ and the shear modulus, $\mu = C_{44}$. The bulk modulus is then given by $B = (C_{11} + C_{12})/2 = \lambda + \mu$ and the Poisson ratio is $\sigma = \lambda/(\lambda + 2\mu)$. The typical error for calculated elastic constants using this type of MD is about 5%.[14] Close to the SSA, large structural fluctuations and slow relaxation lead to errors typically around 10%.

As expected, the bulk modulus decreases very slowly with increasing solute concentration and shows little change at the concentration where amorphization occurs. In contrast, the shear modulus decreases sharply. When the hexatic amorphous phase forms at $x = 0.20$, it plunges more than 50% from the initial shear modulus of the pure, perfect crystalline phase. As a comparison, the measured shear modulus of amorphous phase is usually about 30% smaller than that of the corresponding crystalline phase.[33] Such a large change of shear modulus signals a possible phase transition. The behavior of the Poisson ratio, which is determined mostly by the shear modulus, also increases very rapidly in the concentration range $x = 0.15-0.25$ and levels off in the amorphous region.

This sharp lose of shear elastic rigidity can be understood in terms of the defects present in the binary arrays. *Local atomic position disorder and lattice strain* are two most important contributions from the defects. Since the elastic modulus is related to the long-wavelength part of the strain fluctuations,[34] as more defects are generated, the internal strain fluctuations become larger and the shear elastic modulus becomes smaller. The contributions from the local disorder at the defect cores and their immediate vicinity are relatively complicated. If the fraction of atoms in the defect cores is small, one can, and often does as in continuum mechanics, ignore their contributions to the total elastic modulus. However, this practice is no longer justified if the density is high. These severely deformed regions need to be treated as a ''second phase'' with different (often lower) elastic modulus. The total elastic modulus is, therefore, the weighted average from both disordered and order regions. In addition, dislocation network chains and grain boundaries also contribute to the softening of elastic modulus by changing crystallographic properties of the lattice, such as orientation of the lattice. The misorientation of each crystalline domains can impede sound wave propagation effectively.[35,36]

Since the coupling constant of dislocations depends on the shear elastic modulus,[37] the binding energy of dislocation pairs becomes weaker as the lattice becomes less rigid when more defects are generated. Taking into account of increasing entropy by dispersing single dislocations on 2D, Kosterlitz and Thouless[23] proposed that the dislocation pairs should begin to separate when the dislocation coupling constant decreases below a critical value. The decrease of the elastic shear rigidity of the lattice in turn, makes it easier to generate more defects. Taking this into account, Nelson and Halperin[24] calculated the critical dislocation coupling constants that should reach a universal value of 16π at the hexatic phase formation. Although this result is derived for thermal disordering, it can be applied to other cases including SSA involving stability of dislocation pairs.

In 2D the coupling constant between two edge dislocations with opposite Burgers vectors can be expressed as[23,24,37]

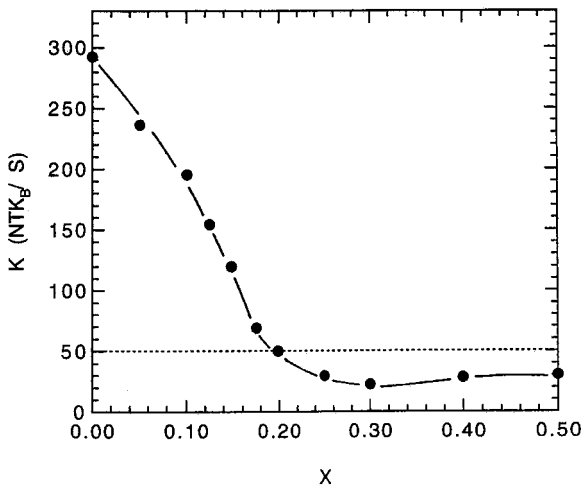

FIG. 10. The dislocation pair coupling constant versus solute concentration for the binary arrays with $\alpha = 0.75$ at $T = 0.2$ and $P = 0.0$.

$$K = \frac{4a^2}{k_B T} \frac{\mu(\mu+\lambda)}{(2\mu+\lambda)}, \tag{17}$$

where a is the lattice spacing of the lattice. Using the Lamé coefficients obtained from the elastic constants, we calculated the coupling constant K as a function of x. As shown in Fig. 10, K exhibits a rapid decline as solute concentration increases. At the hexatic phase transition, it approaches the instability value, 16π, which agrees with our observation that dislocation pairs unbind at the hexatic phase formation. As solute concentration increases further, K levels off and remains almost constant in the amorphous phases.

This behavior is in sharp contrast to that in melting where K remains finite at the melting point and then suddenly drops to zero as the metastable crystalline phase becomes liquid.[9] One can estimate the instability temperature corresponding to $K \rightarrow 16\pi$ by extrapolating the finite K at the melting point to the universal value. It is found that this temperature is well above the equilibrium melting point, and therefore, is the ultimate instability point *inaccessible* to experiments.[9] In contrast, our results show a continuous SSA, or a continuous ''melting'' from a crystalline phase to amorphous phase (frozen liquid), with an intermediate hexatic phase. As discussed below, this is only possible because of kinetic constraint imposed on the system.

5. Kinetic constraint and diffusion

Restricting atoms from executing long-range diffusion in a crystalline solid solution is a necessary condition for the SSA.[1] This polymorphic constraint ensures the following: (1) The disordered crystalline phases do not form equilibrium crystalline phases (which normally occur through long-range diffusion) other than the metastable hexatic and amorphous phases; (2) the compositions remains homogeneous in both the starting crystalline and the final amorphous phase (polymorphic transition); and (3) defects generated by solute atoms are immobile as the consequence of the polymorphic constraint.

Once the defects are created, they are pinned down as long as atoms do not diffuse away beyond several lattice

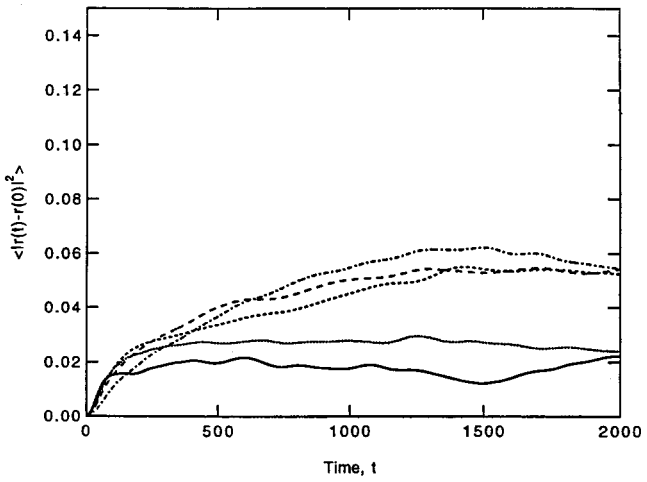

FIG. 11. Time-dependent mean square displacement (MSD) of the binary arrays with $\alpha=0.75$ at $T=0.20$ and $P=0.0$. It is in the unit of σ^2. The solid line is for $x=0.0$, dotted line for $x=0.1$, broken line for $x=0.148$, dashed line for $x=0.199$, and dash-dotted line for $x=0.30$.

parameters. The frozen defects will remain random and homogeneous. Therefore, they have less possibility to form clusters and other defect complexes that can compete and preempty the dislocation unbinding.

This polymorphic constraint is achieved by keeping the systems below the glass transition temperature. In simulations, this is checked constantly by monitoring the dynamic properties of the binary arrays. Figure 11 shows the time dependent mean square displacement for the binary arrays at different solute concentrations. We see that the MSD for all binary arrays reach plateau regions after some initial dynamic relaxations, indicating the absence of long-range diffusion. This is also checked independently by computing the nearest neighbor atom distribution.

6. Atomic displacement

The atomic displacements, as defined in Sec. II, can be used to measure disordering and strength of the strain fields associated with defects. Since the binary arrays are kept below T_g, the dynamic atomic displacements are negligible as compared with the static ones.

Figure 12 shows the static atomic displacement fields of the binary arrays. The arrows are the displacement vectors $\mathbf{u}^s(\mathbf{R}_i)$. For binary array at $x=0.30$, $\mathbf{u}^s(\mathbf{R}_i)$ is magnified by a factor of 2 for ease of viewing. The principal results are summarized below.

First, in crystalline phases the displacements are mainly associated with defects. The largest displacements occur at the cores of the defects with severe disorder around the defects. The displacements show decreasing magnitudes with increasing distance away from the cores. Furthermore, the displacement vectors (or orientations) are highly correlated, especially when the defect density is low. This explains why orientational order (which is related to the nearest neighbor atomic bond orientation), persists longer than the translational order upon displacement of atoms. In particular, we notice that the displacements form vortices with their centers located around the atoms in crystal-like regions. At relatively low solute concentrations, these displacement vortices can be

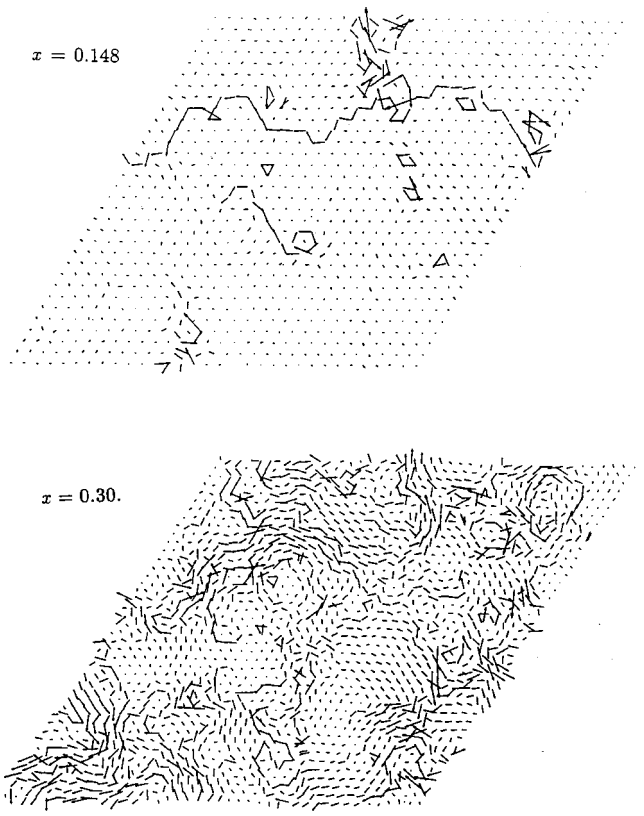

FIG. 12. Static atomic displacement fields for binary arrays with $\alpha=0.75$ at $T=0.2$ and $P=0.0$. The small atoms sometimes cause displacements that are connected to form a long chain. However, it does not lead to topological disorder.

well resolved and thus, the entire sample appears to be partitioned by vortices of various sizes. At higher defect densities, the displacements become less correlated and the displacement vectors are more chaotic. They appear smaller at higher solute concentrations and eventually loose their identity in amorphous phases. By comparing atomic displacement fields and the defect configurations, we are now able to see how defects disrupt the crystalline order and how SSA proceeds. It is the dislocation and dislocation complexes that contribute to the breakdown of translational as well as orientational order.

Second, as more and more defects are generated and more dislocation network chains form, the displacements become inhomogeneous or localized. Most disordering occurs inside the (existing) dislocation network chains, especially when the solute concentrations are high.

The degree of disordering can be estimated by the static mean square displacements (SMSD) using Eq. (16). As shown in Fig. 13, it changes continuously with increasing solute concentration and shows no abrupt increase before the onset of the hexatic phase formation at $x=0.20$. This increase slows down when the binary array becomes amorphous. This behavior is in sharp contrast to that of the mean square dynamic displacement at melting where the MSD shows a sudden jump and then diverges due to onset of *diffusion* at melting.

Third, from the displacement fields one can perceive the strain fields in the disordered crystalline binary arrays. The strain field $\epsilon_{\alpha\beta}(r)$ is proportional to the derivatives of the

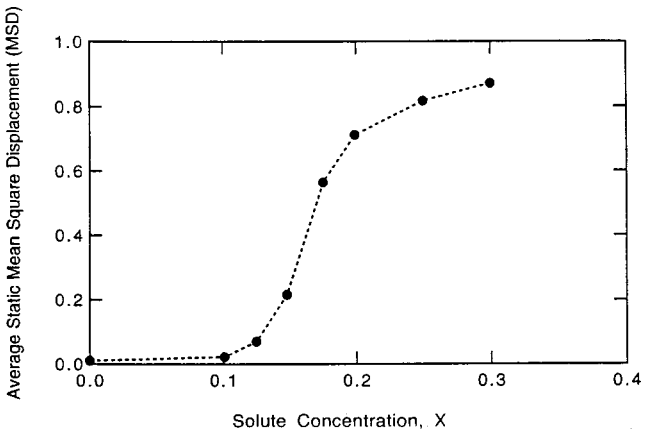

FIG. 13. Mean square static displacement for the binary arrays with $\alpha=0.75$ at $T=0.2$ and $P=0.0$.

displacement vectors, $\epsilon_{\alpha\beta}=1/2[\partial_\alpha u_\beta(\mathbf{r})+\partial_\beta u_\alpha(\mathbf{r})]$. As shown in Fig. 12, the varying displacement vectors in different parts of the sample indicate that the strain fields associated with defects are highly inhomogeneous. As more defects are introduced, the correlation of atomic displacements over distance decreases, resulting in short ranged strain fields. The presence of an internal strain field not only contributes directly to the increase of the free energy for the disordered crystalline binary arrays, but also to the decrease of elastic shear modulus.

7. Density

Figure 14 shows the molar density of the binary arrays versus solute concentration. The density shows three distinctive regions, with nearly linear density changes in each region. The first region ($x<0.05$) is the equilibrium binary solute solutions. The increase of the density is caused mainly by addition of smaller solute atoms to replace larger solvent atoms. Of particular interest is the density change across the hexatic phase transition. There is no significant change in the molar density from the crystalline phase to the hexatic amorphous phase; only slopes at two sides of the density are different.

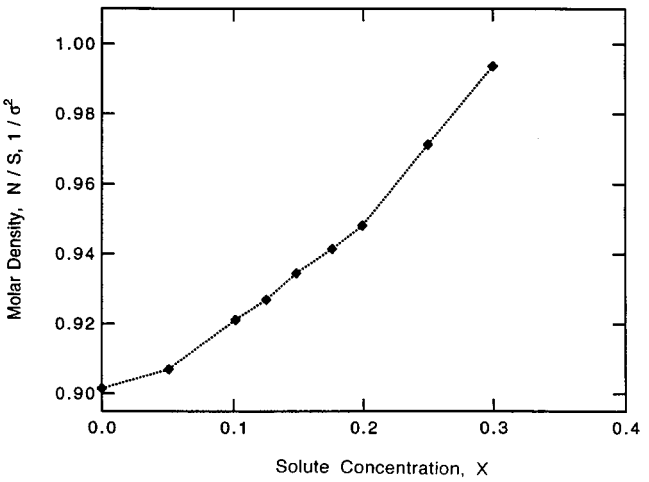

FIG. 14. Molar density of the binary arrays with $\alpha=0.75$ at $T=0.20$ and $P=0.0$.

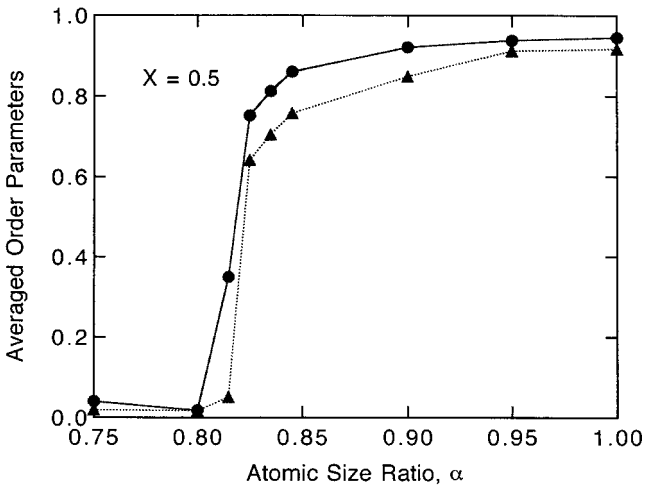

FIG. 15. The order parameters for binary arrays with $x=0.50$ at $T=0.20$ and $P=0.0$. The triangles are for the average local translational and the filled circles are for the orientational order.

The nearly continuous molar density change across the crystalline-hexatic amorphous phase boundary implies that under isothermal ($\delta T=0$) and polymorphic ($\delta x_i=0$, $i=A,B$) conditions, the entropy change of the binary arrays between the crystalline phase and the hexatic amorphous phase is small.[38] It appears that the binary array undergoes the transition with very small latent heat, which is in sharp contrast with that of ordinary melting.

Similar results are observed for the molar enthalpy. The molar enthalpies of both crystalline and amorphous phase, as extrapolated to the critical composition of the hexatic phase, change only slightly. The molar enthalpy of the amorphous phase remains nearly constant with further increase of the solute concentration. This slow response to solute addition (also observed in the elastic properties) is a general characteristic of the amorphous phase.

B. Binary arrays with (0.50, α) at $T=0.20$, $P=0.0$

The model system is the equimolar binary arrays with solute concentration fixed at $x=0.50$ with $T=0.2$ and $P=0.0$. The computation procedure for this model system is the same as that used in the previous case, except that the variable is the atomic size ratio, α. Similar equimolar binary arrays was investigated by Bocquet *et al.*,[39] who studied the amorphization transition induced by atomic size differences in the binary solution with pure repulsive interatomic interactions. They reported a first order SSA transition. In the following, we summarize the principal results for the model binary array with LJ potentials using constant pressure and temperature MD.

Our simulation shows a quantitatively different RDF which resembles that of a liquid at the critical atomic size ratio, $\alpha_c=0.825$. Both local translational and orientational order parameters, as shown in Fig. 15, vanish at the critical atomic size ratio. This is quantitatively different from that of the binary arrays at the fixed atomic size ratio in Fig. 4. Correspondingly, as α_c is approached, both order correlation functions rapidly decay to zero at the same rate at about the third nearest neighbor distances.

Furthermore, the number of the total disclination defects, as shown in Fig. 16, is negligible at atomic size ratios larger

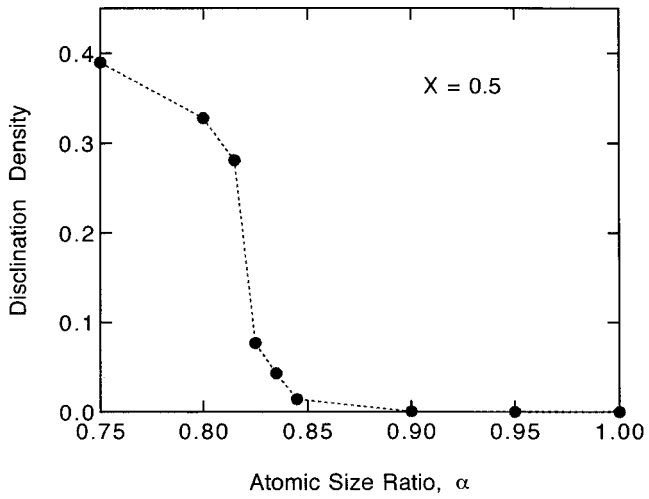

FIG. 16. Average defect density for the binary array with $x = 0.50$ at $T = 0.2$ and $P = 0.0$.

than 0.845 where crystalline phases are stable. It then rises abruptly to about 25% when the binary array becomes amorphous at α_c. The defect configuration reveals that the defects are composed predominantly of 5- and 7-nearest neighbor disclinations. At the critical α_c, however, the dislocation pairs do not form isolated dislocation singlets or dislocation network chains. Instead, they form large dislocation aggregates. The dislocation pair coupling constant, K, remains finite in the crystalline phase slightly above α_c and shows a discontinuous drop at the transition as reflected in the shear modulus (see Fig. 17). These results lead us to the conclusion that the hexatic amorphous phase is no longer present when the crystalline phase is destabilized. The crystal to glass transition appears to be first order, which agrees with the results reported in Ref. 38.

This conclusion is further supported by thermodynamic and elastic properties of the binary arrays: The shear elastic modulus does not decrease continuously with α across the crystalline/amorphous phase boundary. It drops abruptly, at $\alpha = 0.825$ (Fig. 17). Similar behavior is observed in ordinary

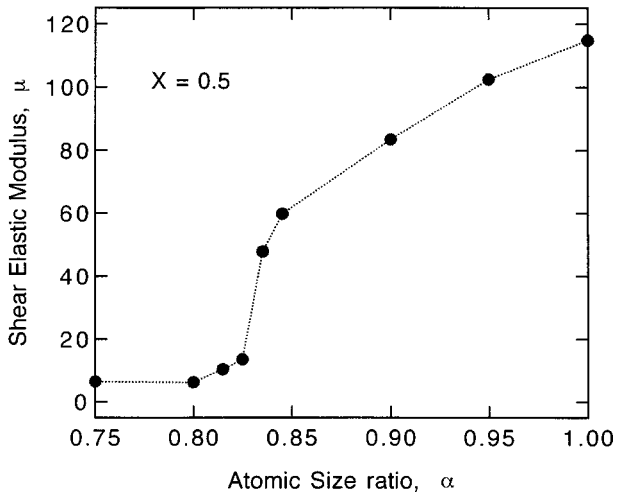

FIG. 17. Isothermal shear elastic constant versus solute-solvent atomic size ratio in the binary arrays with $x = 0.50$ at $T = 0.20$ and $P = 0.0$.

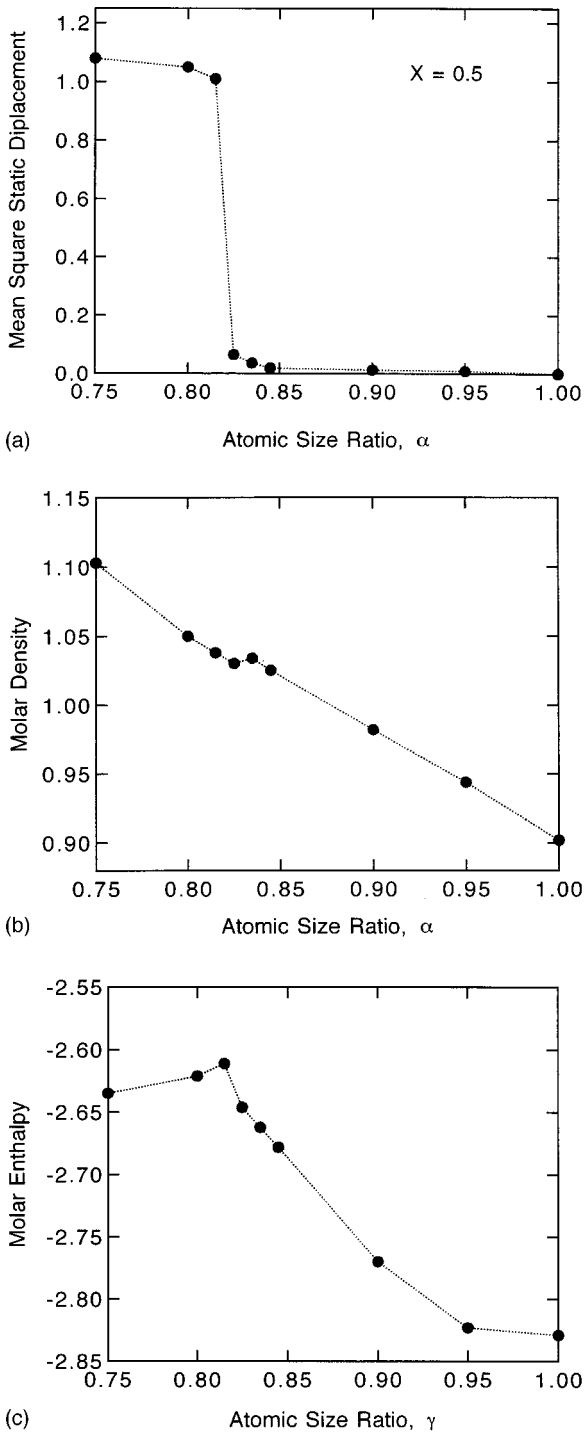

FIG. 18. (a) Mean square static displacement, (b) molar density, and (c) molar enthalpy, for the binary arrays with $x = 0.50$ at $T = 0.2$ and $P = 0.0$.

melting.[9,13] The static mean square displacements, molar density, and molar enthalpy also exhibit the same discontinuous change at the transition (Fig. 18), indicating a first order transition.

IV. DISCUSSION

The results from above two case studies demonstrate that dislocations and dislocation complexes play a crucial role in the SSA in 2D crystalline solids. For binary substitutional

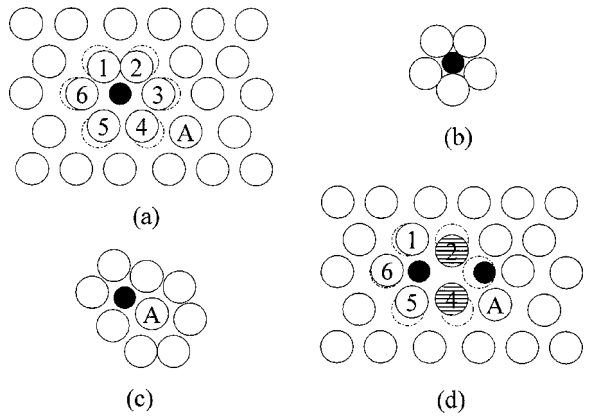

FIG. 19. The schematics of the local disorder, or symmetry breaking, induced by dislocation pairs when small solute atoms are added (see Fig. 7 for detailed atomic defect configurations). (a) Addition of a solute atom (the filled circle) with size difference causes position disorder for surrounding solvent atoms. (b) Five nearest neighbors are preferred geometrically for solute atom 25% smaller in radius (Ref. 40). (c) But a seven nearest neighbor ring for solvent *A* also needs to be created to maintain the overall mean nearest neighbors at six. The energy associated with this 5–7 dislocation is too high to allow this to happen. Thus the sixfold local symmetry is intact. (d) If a second solute is added to substitute one of the nearest neighbor solvents of the original solute (the number 3 solvent), a dislocation pair made of two 5- and 7-nearest neighbor disclination pairs are created (the two solutes and the number 2 and 4 solvents). As a result, the fair-field distortion and strain field are canceled.

arrays, these defects are clearly seen to be generated by atomic size difference. The insights we learned from this work helps delineating the role of the atomic size difference that plays in the atomic size induced topological-order-to-disorder transitions in 2D. In the following, we discuss the underlying mechanisms.

A. Coordination number change, dislocation formation, and symmetry breaking

The direct consequence caused by the size difference is the change in interatomic interactions among the atoms within the cut-off distance of the interatomic potentials [Eqs. (1a) and (1b)]. If one replaces the solvent atoms by solutes, the big solvent atoms would relax toward the small solute atoms as the large solvent is sitting at the position in the solvent-solute interatomic potential that has a negative slope. This results in position displacements of the surrounding solvent neighbors. The displacement field is symmetric centered around the solute atom [Fig. 19(a)], making it appear that the solute is under a hydrostatic pressure. From a pure geometric point of view, if the solute atom is small enough, such as in our case (25% smaller), the solute would prefer to have only five bigger solvent atoms as its nearest neighbors [Fig. 19(b)]. The neighboring solvents in this case would form a closed ring, leaving no extra space around the small solute. This change in coordination number is thought to be driven by the hydrostatic pressure resulting from the atomic volume disparity between the small and big atoms.[40] The small solute, which has more space surrounding it upon being placed on the position occupied previously by the large solvent, appears under tension while the solvents are under compression. This simple argument led to the theory[40] predicting that if the atomic size difference reaches a critical value, the pressure surrounding the solute would cause the local (extra) space to collapse. As a result, the original six nearest neighbors of the solute become five. The topological instability of the local structure or symmetry is therefore proposed as the mechanism resulting from the change of the nearest neighbor coordination shell. According to this theory, the 5- and 7-nearest neighbor coordination number defects in the 2D binary array should form when the atomic size ratio reaches 25% as a result of the local coordination number change, or fluctuation induced by the hydrostatic pressure due to atomic size disparity.[40] As discussed below, there is a crucial piece that is missing in this theory in assessing the energy barriers to form such a defect. As a result, this proposition may need to be reconsidered for topological order-to-disorder transitions or SSA in two dimensions.

Since the mean coordination number in the 2D hexagonal lattice is six, if the small solute has five neighbors, one of its neighbors must have seven nearest neighbors. Therefore, creating a dislocation with a 5–7 nearest neighbor coordination number (disclination pair) is equivalent to squeezing the small solute atom into the 6 member ring of the nearest neighbor solvents of the solvent atom A that is the next nearest neighbor to the solute atom [see Figs. 19(a) and 19(c)]: This 7-nearest neighbor defect needs to be created to maintain the mean coordination number at six. One possible way to accommodate the solute atom which is 25% smaller is for the six nearest neighbor solvent atoms of A to move outward a distance about 20% of the radius of the central solvent atom A to open up a 45.2° gap in the nearest neighbor ring [Fig. 19(c)]. This operation, however, requires a 40% area expansion, and may be too costly energetically. Therefore, although the geometric packing favors the 5-nearest neighbor arrangement around the small solute, a 7-nearest neighbor configuration also needs to be created. This corporative arrangement around the two atoms, which is not accounted for from a pure geometric point of view,[40] requires a relatively high energy associated with the local area expansion.

If this high cost of energy alone is not sufficient to prevent the 5- and 7-nearest neighbor coordination defect from forming, the additional increase in the energy barrier can certainly prohibit its formation. The additional energy is contributed from the long-range strain field of this defect: The highly correlated defect configuration is an edge dislocation in 2D.[19–21] The energy associated with creating the aforementioned 7-neighbor coordination defect is simply a *local* event at the dislocation core; the additional energy arising from the *long-range* strain field of the single dislocation made of a pair of 5- and 7-nearest neighbor disclinations is a result of a *nonlocal* event. As is known,[21,37] its energy is divergent. Therefore the probability to form such a single dislocation is extremely low. Indeed, our results show that there are almost no 5–7 disclination pairs, or single dislocations to form (Fig. 7). The very few ones that do show up as shown in Fig. 7(a) are only the transient ones. They either disappear after some short period of time, or combine with other dislocations nearby. Therefore, we conclude that distortion from a *single* solute atom alone is not sufficient to

break the sixfold symmetry, even when the atomic size difference is close to or above the critical size ratio in the 2D binary array for topological/geometric instability.[40]

However, if one can substitute one of the nearest neighbor solvent atoms of the first solute by another solute atom [see Fig. 19(d)], an additional 5–7 disclination pair can be created by slightly rearrangement of the neighbors using the extra space created around the second solute. This new 5–7 disclination pair is the immediate neighbor of the existing 5–7 disclination pair. As a result, a *dislocation pair* is created. As is known,[21,37] the dislocation pair has much lower strain energy as compared with the single dislocation due to the cancellation of the long-range strain field. It can be seen clearly in Fig. 7 that the defects are indeed composed mostly of two 5- and 7-nearest neighbor dislocation pairs. As illustrated in Fig. 19(d) as well as in Fig. 7, the far-field distortion around the dislocation pair, which is usually manifested as extra atomic lines and curved atomic lines, is virtually absent. Therefore, both the *local atomic position displacement disorder*, which leads to the formation of dislocation cores, and their *long-range strain fields* in the lattice need to be considered in evaluation of the coordination number change. In other words, the atomic size mismatch alone is not sufficient to break the six-fold symmetry in 2D. It requires a corporative arrangement of a number of atoms, two neighboring solutes and their solvent neighbors, to accomplish the job.

B. Continuous crystal-to-amorphous transition

The phase diagram in Fig. 1 shows different phases corresponding to different regions of atomic sizes and solute concentrations. When atomic size difference is large (slightly below the critical size difference, α_c), the transitions are continuous as solute concentration changes. There is an apparent intermediate hexatic phase bridging the crystalline phase and the true amorphous phase. On the other hand, at the high solute concentration (close to equimolar point), the intermediate hexatic amorphous phase does not exist and the thermodynamic properties show a discontinuous change when the critical atomic ratio is traversed. There is an apparent critical point where the discontinuous crystal-to-amorphous transition becomes a continuous transition. We attribute this difference to the strain field present in the system under the polymorphic and kinetic constraints. In the second part of this work, we will present a theoretical model to explain this crossover phenomenon.[41]

In the case of continuous SSA, when the atomic size difference is larger than the critical one (but not too large to form compound and short-range ordering), the defect density is largely controlled by the randomly distributed solutes. The defect density increases continuously with the increase of solute concentration, but the polymorphic constraint prevents the defects from migrating too far. They remain scarce in the crystalline phases and interact with long range strain fields. As the hexatic phase is approached, the paired dislocations tend to unbind to form hexatic phases as driven by the decreasing elastic shear modulus and the increasing entropy contributed by the isolated dislocations. At higher dislocation density, strong interactions between dislocations leads to formation of dislocation network chains, a precursor of small angle grain boundaries.[21] The true amorphous phase forms when dislocations become aggregated at higher defect density.

For the binary arrays close to the equimolar concentration, the high solute density provides the basis for generating a large number of defects. When the atomic size difference reaches the critical atomic size difference, defects are generated spontaneously. This overwhelmingly large number of defect become clustered immediately,[42] preemptying formation of the hexatic amorphous phase.

C. Solid state amorphization and melting

These findings shed light on the topological order-to-disorder transition in general. In particular, we would like to point out the difference between melting and solid-state amorphization.

Following the path of alloying at low temperature, we can control the defect density to make the binary arrays approaching the conditions specified by Kosterlitz and Thouless.[23] This advantage is virtually absent in the case of thermal melting. Since dislocations in these systems are generated by thermal vibrations as the crystal is heated, the defect density is determined by both temperature and the interatomic potentials (closely related to the defect formation energy). A large number of defects are generated at the melting temperature due to large-amplitude vibrations.[9,43] Furthermore the lattice strain associated with the defects is relaxed quickly through thermal vibration. Even more significant is the defect clustering driven by defect interactions and further facilitated by diffusion. At an elevated temperature close to melting point, dislocations are able to move rapidly with the assistance of atomic diffusion to form lower energy configurations such as grain boundaries and dislocation aggregates.[9,44] Since dislocation pair unbinding can occur only when dislocations are relatively scarce and there are no dislocation complexes such as grain boundaries,[23] presence of the overwhelmingly large numbers of clustered dislocations can preempt the pair unbinding.[44] These defect aggregates become seeds for nucleation and subsequent growth of liquid phases.

Our work also provides microscopic details missing in the early proposition for the SSA.[40] As our work has shown, the topological disorder, as observed in the 2D model solid solution, is the direct consequence of the strongly correlated stress (or strain) fields originating from the local distortions around the solute atoms. *Isolated solutes alone cannot break the local symmetry*, even though the atomic size difference is close to the critical value.[40] The (far-field) stress field associated with different sized atoms, which is considered to be hydrostatic compression and tension stress only,[40] does not vanish by simply changing of their coordination numbers. The unique relationship between the coordination number defect and dislocation in 2D requires more intricate arrangement of atoms and their coordination numbers. It is the corporative efforts involving a group of atoms, as dictated by the interacting strain fields, that eventually result in breaking the local order. This is evidenced by the formation of the dislocation pairs and their complexes in our simulations.

Our work also indicates that it is the shear stress (field) arising from the dislocations, not the hydrostatic pressure caused by the atom volume difference for different sized

atoms,[40] that is responsible for the local topological instability, or nearest neighbor coordination number change. The direct evidence from the present work shows that there are more space created when dislocation pairs form. Instead of reducing the space surrounding the solute presumably under the hydrostatic (tension) pressure generated by atomic size difference[40] the space surrounding the two 7-nearest neighbor disclinations and the 5-nearest neighbor disclinations in a dislocation pair become even bigger due to the inefficient packing. The molar volume around the solute atom in the dislocation pair is larger than that surrounding the same solute before relaxation takes place in the initial crystalline lattice (see Fig. 7). The extra space, or free volume,[46] is created, even with an increase of (local) energy, as the result for the system to lower its (long-range) strain energy arising from single dislocations. The later is prohibitively large, but becomes much smaller when two single dislocation combine to form dislocation pairs. The extra space remains stable as long as the dislocation pairs are present.

V. CONCLUSION

It has been a general belief starting with Born[1–4,45] that the elastic shear instability is a cause of crystalline instability. This idea has been used to explain the SSA.[1,4] However, it is known that this model is not adequate to provide information on what the resulting phase should be when the instability is reached and how the transition is related to microscopic structures and defects. Another proposition is that melting, as well as SSA, could not be continuous because of absence of the symmetry relation between the topologically ordered and disordered phase. Although KTNHY theory predicts an alternative mechanism, an overwhelmingly large amount of work,[44] especially that from computer simulations,[9,14,15] appear to preclude such a transition. Despite the simplicity of the model system, our work shows unambiguously that crystalline instability is caused by various topological defects; and most importantly, the transition could be continuous. As shown, the crystalline defects contribute directly to atomic position disorder and lattice strain. It is the interplay of the two that leads to softening of elastic modulus and final collapse of the crystallinity.

As demonstrated in the two examples for binary arrays, transition from crystalline phase to amorphous phase is closely related to defect properties and the kinetic constraints. If the dislocation density is low and dislocations are pinned by solute atoms, the transition could be continuous with an intermediate hexatic phase. However, if the number of dislocations are high and they form clusters, the transition is abrupt. Since defect complexes are energetically favored as defect density increases, collective defects such as dislocation network chains, grain boundaries, and dislocation clusters start to play a more important role in disrupting crystalline order than the elemental defects do. If the distribution and mobility of defects can be controlled by kinetic constraints, the topological ordered phase can undergo a continuous transition to the disordered one.

As a final note, a great caution needs to be taken to generalize the results to three dimensions. There are several key connections that are missing when one goes from 2D to 3D. The first is that it is not obvious how the extended defects such as disclination, dislocation, and grain boundaries are related to solute atoms, or point disorder. The questions of whether or not the solute-induced topological defects exist and if they do, how to characterize them remain to be answered. The second is the diminishing role of the thermal fluctuations from 2D to 3D. This may make it more difficult to destabilize the crystallinity in 3D. Finally, the contribution of entropy from dislocations to destabilization of crystalline order is much less in 3D, which may lead to disappearance of the hexatic phase and also the continuous topological order-to-disorder transition manifested by it.

ACKNOWLEDGMENTS

The author would like to thank W. L. Johnson and W. A. Goddard for their encouragement and support. He also thanks N. Q. Lam, P. R. Okamoto, and H. J. Fecht for many stimulating discussions. The support for this work was provided partially by the start-up fund from the Whiting School of Engineering at The Johns Hopkins University and from the Department of Energy (DE-FG02-99ER45784).

[1] W. L. Johnson, Prog. Mater. Sci. **30**, 81 (1986).
[2] K. Samwer, H. Fecht, and W. L. Johnson, in *Glassy Metals III*, edited by H.-J. Günthrodt and H. Beck (Springer-Verlag, Berlin, 1994).
[3] P. R. Okamoto, N. Q. Lam, and L. E. Rehn, Solid State Phys. **52**, 1 (1999).
[4] M. Li and W. L. Johnson, Phys. Rev. Lett. **70**, 1120 (1993).
[5] L. J. Talon, Nature (London) **342**, 658 (1989).
[6] M. Iwamatsu, J. Phys.: Condens. Matter **11**, L1 (1999).
[7] J. Daeges, H. Gleiter, and J. H. Perepezko, Phys. Lett. A **119**, 79 (1986).
[8] H. J. Fecht and W. L. Johnson, Nature (London) **334**, 50 (1988).
[9] F. F. Abraham, Phys. Rep. **5**, 339 (1981).
[10] M. Born, J. Chem. Phys. **7**, 591 (1939).
[11] N. Q. Lam and P. R. Okamoto, MRS Bull. **19** (7), 41 (1994); see other references therein.
[12] F. A. Lindemann, Z. Phys. **11**, 609 (1910).
[13] A. R. Ubbelohde, *Melting and Crystal Structure* (Clarendon Press, Oxford, 1965).
[14] K. J. Strandburg, Rev. Mod. Phys. **60**, 161 (1988).
[15] M. A. Glaser and N. A. Clark, Adv. Chem. Phys. **83**, 543 (1993).
[16] F. H. Stillinger and A. Rahman, J. Chem. Phys. **57**, 1281 (1972).
[17] M. Li and W. L. Johnson, Phys. Rev. B **46**, 5237 (1993).
[18] M. Li, W. L. Johnson, and W. A. Goddard, in *Materials Theory and Modeling*, edited by J. Broughton, P. Bristove, and J. Newsam, MRS Symposia Proceedings No. 291 (Materials Research Society, Pittsburgh, 1993), p. 285.
[19] W. L. Bragg and J. F. Nye, Proc. R. Soc. London, Ser. A **190**, 474 (1947); Y. Ishida and S. Iyama, Acta Metall. **24**, 417 (1976).
[20] J. P. McTague, D. Frenkel, and M. P. Allen, in *Ordering in Two Dimensions*, edited by S. K. Shinha (North-Holland, Amsterdam, 1980).

[21] D. Hull and D. J. Bacon, *Introduction to Dislocations*, 2nd ed. (Pergamon, Oxford, 1984).
[22] W. Fisher and E. Kock, Z. Kristallogr. **150**, 245 (1979).
[23] J. M. Kosterlitz and D. J. Thouless, J. Phys. C **6**, 1181 (1974); J. M. Kosterlitz, *ibid.* **7**, 1046 (1974).
[24] D. R. Nelson and B. I. Halperin, Phys. Rev. B **19**, 2457 (1979); **21**, 5312 (1980).
[25] A. P. Young, Phys. Rev. B **19**, 1855 (1979).
[26] For recent work, see J. Lee and K. J. Strandburg, Phys. Rev. B **46**, 11 190 (1992); J. A. Zollweg and G. V. Chester, *ibid.* **46**, 11 186 (1992).
[27] *Bond-Orientational Order in Condensed Matter Systems*, edited by K. J. Strandburg (Springer-Verlag, New York, 1992).
[28] D. R. Nelson, M. Robinstein, and F. Spaepen, Philos. Mag. A **46**, 105 (1982); M. Robinstein and D. R. Nelson, Phys. Rev. B **26**, 6254 (1982).
[29] K. J. Strandburg, J. A. Zollweg, and G. V. Chester, Phys. Rev. B **30**, 2755 (1984).
[30] J. Y. Wong and G. V. Chester, Phys. Rev. B **35**, 3506 (1987).
[31] M. Li, W. L. Johnson, and W. A. Goddard, Phys. Rev. B **54**, 12 067 (1996).
[32] E. J. Jensen, W. Damgaard Kristensen, and R. M. J. Cotterill, Philos. Mag. **27**, 623 (1973).
[33] H.-U. Künzi, in *Glassy Metals II*, edited by H.-J. Günthrodt and H. Beck (Springer-Verlag, Berlin, 1983).
[34] L. D. Landau and E. M. Lifshitz, *Theory of Elasticity*, 3rd ed. (Pergamon, Oxford, 1986).
[35] R. F. S. Hearmon, Adv. Phys. **5**, 323 (1956).
[36] F. Stanke and G. S. Kino, J. Acoust. Soc. Am. **75**, 665 (1984).
[37] J. P. Hirth and J. Lothe, *Theory of Dislocations*, 2nd ed. (Wiley, New York, 1982).
[38] H. B. Callen, *Thermodynamics and An Introduction to Thermostatistics*, 2nd ed. (Wiley, New York, 1985).
[39] L. Bocquet, J.-P. Hansen, T. Biben, and P. Madden, J. Phys.: Condens. Matter **4**, 2375 (1992).
[40] T. Egami, Mater. Sci. Eng., A **226**, 261 (1997); and references therein.
[41] M. Li (unpublished).
[42] The continuum percolation threshold in two dimensions is 0.45 beyond which the clusters are connected, see R. Zallen, *The Physics of Amorphous Solids* (Wiley, New York, 1983), pp. 183–191.
[43] J. Tobochnik and G. V. Chester, Phys. Rev. B **25**, 6778 (1982).
[44] S. T. Chui, Phys. Rev. B **28**, 178 (1979).
[45] J. T. Tallon, Philos. Mag. A **39**, 151 (1979); J. T. Tallon and W. H. Robinson, Philos. Mag. **36**, 741 (1977).
[46] D. Turnbull and M. H. Cohen, J. Chem. Phys. **31**, 1164 (1959); **34**, 120 (1961).